Inviscid and viscous CFD modeling of plume dynamics in laser ablation

Kedar A. Pathak, Alex Povitsky*

Department of Mechanical Engineering, University of Akron, Akron, OH 44325, USA

Abstract

We model the dynamics of a laser ablated plume in production of carbon nanotubes using computational fluid dynamics techniques. A higher-order ENO scheme is used for modeling the plume. The exact physical phenomenon of laser ablation plume dynamics is comparatively complex. For simplicity we model the plume and surrounding laser furnace gas as a single-species ideal gas. We are aiming at capturing the basic features of a laser ablated plume that will help in future to control the plume's evolution using simplified models. We solve Euler equations, Navier-Stokes equations, and Navier-Stokes equations with an appropriate model of the turbulent flow field. A Euler equations-based model appears to be adequate for first dozens of microseconds. For modeling of several hundreds of microseconds after the ablation, the viscous terms are needed to model the plume's diffusion. For millisecond-range modeling, the influence of unsteady turbulent flow in the laser furnace may become significant. The baroclinic and viscous deposition of vorticity on the plume is obtained numerically and the interaction of the plume with reflected shock waves appears to be the major source of the deposited vorticity. In this paper, a relatively simple analytical model of dynamics of plume will be discussed. This model will be based on evaluation of vorticity on the plume and formation of the vortex couple.

Keywords: Laser ablation; Plume gas dynamics; Vorticity deposition; ENO schemes

1. Introduction

In application of high-intensity lasers to material processing, the formation of an ablated plume and its dynamics are of high importance. In general, the ablated plume is a multi-phase flow and may contain solid particles and liquid clusters of molecules. Nevertheless, the plume dynamics shows well-defined gas dynamic effects [1]. As the ablation plume expands and interacts with the background gas, local distributions of particles velocities eventually evolve towards Maxwellian ones, allowing for application of gas-dynamic continuous computational models. Long-term plume evolution in a near-atmospheric pressure background gas can be well described by continuous gas dynamics. In most of processes for synthesis of nanotubes, the nanosecond laser pulses are applied to the target and the injection velocity of plume is supersonic. Experiments by Puretzky et al. [2] have shown that the initial gas pressure in the ablated plume can exceed 100 atm that in turn, produces shock in the ambient gas. In turn, the propagation of incident and reflected shock waves in a confined space of laser furnace affect the plume behind the incident shock wave. Before the shock wave hit the side wall of the furnace, its propagation is adequately described by the self-similar analytical solution [3,4]. At later time moments, the furnace chamber confines the plume and produces reflected shock waves that are difficult or impossible to account for in existing analytical models. These reflected shock waves are crucial for plume dynamics since the interaction of plume with reflected shock waves contributes to baroclinically generated vorticity. In turn, this deposited vorticity determines the formation of vortex couple that controls the plume evolution in the later stages of plume development. Temperature and dynamics of the emitted plume catalyst particles are crucial for modeling the growth of nanotubes deposited on these catalyst particles. The previously developed plume dynamics model by Lobao et al. [5,6] has been based on compressible multi-species Euler equations written in general curvilinear coordinates. The goal of their model was to obtain the temperature of catalyst particles as a function of time, show the influence of

* Corresponding author, Tel.: +1 (330) 972 2685; Fax: +1 (330) 972 6027; E-mail: povitsky@uakron.edu

Computational Fluid and Solid Mechanics 2005
K.J. Bathe (Editor)

chamber pressure, injection velocity, and periodicity of the plume on the temperature of particles, and discuss physical reasons for non-monotonic temperature behavior of catalyst particles. This temperature as a function of time is needed to model chemical reactions leading to the nucleation of nanotubes.

The effective viscous length-scale can be defined as $\ell_{\text{visc}} = \sqrt{\nu\tau}$, where ν is effective viscosity and τ is the time-scale of the modeled phenomena. This method to evaluate the influence of viscous forces has been used by Quirk et al. [7] and other papers dealing with the shock wave interactions with isolated flow inhomogeneities. This criterion is based on analytical solution for the penetration of boundary layer into the fluid in rest due to the impulsive motion. For example, in the laser ablation model in synthesis of carbon nanotubes [5] the considered time interval was $200\,\mu$s and the viscous length-scale is $\ell_{\text{visc}} \sim 100\ \mu$m. This length-scale is two orders of magnitude smaller than the cross-section of the plume and, therefore, the viscous effects seem to be negligible for such a time interval. On the other hand, the model of plume dynamics by Greendyke et al. [8] is based on the Reynolds-stresses model of turbulence and includes adjustment of plume initial conditions to laser ablation experiments by Puretzky et al. [2]. The choice between inviscid, viscous, and turbulent models for plume dynamics is not straightforward since the highly compressible ablated plume undergoes several interactions with shock waves, and the above-listed simplified criterion may not be adequate.

Furthermore, the modeling of multiple plume injection as a result of laser ablation is important for large-scale production of carbon nanotubes where the laser hits the target many times within a short period [5]. In the limit case of a very short time between two consecutive pulses, the under-expanded jet analogy is used by Bulgakov et al. [9] to predict the effect of plume focusing and vortex formation. The choice between inviscid and viscous models will become more sophisticated than that for single plume.

In the current paper we compare our computational results obtained by inviscid and viscous models for plume dynamics. We study the shock-plume interaction numerically and will present a simplified analytical model for plume evolution based on evolving of deposited vortex pair.

2. Governing equations and numerical methods

The governing equations are the two-dimensional unsteady compressible Navier-Stokes equations. The conservative equations are given by

$$\frac{\partial U}{\partial t} + \frac{\partial F}{\partial x} + \frac{\partial G}{\partial y} = \frac{\partial R}{\partial x} + \frac{\partial S}{\partial y} \tag{1}$$

where,

$$U = \begin{bmatrix} \rho \\ \rho u \\ \rho v \\ \rho E \end{bmatrix},\ F = \begin{bmatrix} \rho u \\ p + \rho u^2 \\ \rho uv \\ (p + \rho E)u \end{bmatrix},\ G = \begin{bmatrix} \rho v \\ \rho uv \\ p + \rho v^2 \\ (p + \rho E)v \end{bmatrix}$$

$$R = \begin{bmatrix} 0 \\ \tau_{xx} \\ \tau_{xy} \\ u\tau_{xx} + v\tau_{xy} - q_x \end{bmatrix},\ S = \begin{bmatrix} 0 \\ \tau_{yx} \\ \tau_{yy} \\ u\tau_{yx} + v\tau_{yy} - q_y \end{bmatrix}$$

the state equation for an ideal gas in thermodynamic equilibrium can be written as

$$\frac{p}{\rho} = (\gamma - 1)\left(E - \frac{u^2 + v^2}{2}\right) \tag{2}$$

Since the flow field involves shock waves and smooth areas of flow field, we use the Essentially non-oscillating (ENO) scheme as given by Shu [10] to discretize the non-linear terms in above equations. The ENO scheme not only discards the stencil giving the oscillations in the flux, but also chooses the smoothest stencil. The choice is made using the Newton divided difference. After choosing the smoothest stencil, reconstruction is done to find the numerical flux function at the cell interface. The numerical flux function

$$\hat{f}_{i+\frac{1}{2}} = \hat{f}(f_{i-r}, \ldots, f_{i+s}), \quad i = 0, 1, 2, \ldots, N \tag{3}$$

is calculated using the stencil chosen by ENO scheme with the following k points:

$$x_{i-r}, \ldots, x_{i+s} \tag{4}$$

where $r + s = k - 1$. The numerical flux function $\hat{f}_{i+\frac{1}{2}}$ is expressed as

$$\hat{f}_{i+\frac{1}{2}} = \sum_{j=0}^{k-1} c_{rj} f_{i-r+j} \tag{5}$$

where the constants c_{rj} are given by Shu [10].

We study the plume evolution during a time period of the order of a single millisecond, which is comparable to the lifetime of a few turbulent eddies. Therefore, the turbulence in the flow is modeled in the following way: First, the turbulent kinetic energy and the rate of dissipation are calculated using the 3%-level of turbulence in the laser furnace:

$$u' = .03u,\ K = \frac{3}{2}u'^2,\ \epsilon \frac{c_\mu K^{\frac{3}{2}}}{\ell} \tag{6}$$

where $\ell = 0.1D$, and D is the diameter of the laser

furnace. Next, using the discrete random model employed by Povitsky et al. [11], the average lifetime of turbulent eddies is calculated as

$$t = c\frac{K}{\epsilon} \tag{7}$$

This provides the semi period in the space of the eddies, which is

$$L = ut \tag{8}$$

As a first guess, the initial turbulent gust can be set as

$$u' = u'_{max}\sin(\frac{\pi}{L}x) \tag{9}$$

and adding a proper phase shift along the vertical direction, we get a gust-type turbulent flow-field.

3. Results and discussion

Solutions for an ablation plume are presented at post-ablation time of 300 μs (see Fig. 1). The plume rapidly disperses into the base flow and evolves into a downwards-moving vortex pair.

When viscous effects are included, the plume shape agrees satisfactorily with the experimental shadow photos [12]. Some difference between experimental and simulation results can be attributed to fact that the real plume in actual carbon nanotube synthesis involves multiple species of carbon, as against the single-species ideal gas in the present study. The effect of the turbulent gust is minor at the considered time interval of 300 μs.

It is possible to develop an analytical model that determines the plume shape from the amount of deposited vorticity. Such a model could be viewed as an extension of the shock–bubble interaction by Yang et al. [13]. This model can be used to predict the behavior of the plume through vorticity dynamics – baroclinic and viscous vorticity deposition on the plume. The current problem is significantly more involved than the single shock wave–bubble interaction since the plume interacts with several oblique shock waves and possibly with expansion waves.

Following Yang et al. [13], extensive numerical simulations for various initial conditions are needed to validate such a simplified model. The behavior of the vortex pair that, in turn, controls the plume evolution can be analyzed using the vorticity transport equation:

$$\frac{D\omega}{Dt} = \omega\cdot\nabla q + \nu\nabla^2\omega + \frac{\nabla\rho\times\nabla p}{\rho^2} \tag{10}$$

In the above equation the cross product of the density and pressure gradient is the baroclinic vorticity source. The density gradient exists inside the plume and the strong pressure gradient is provided by reflected shock waves of the incident shock wave. This gives rise to vorticity generation inside the plume. The source of vorticity about one of the vortical structures is shown in Fig. 2(a). It is calculated by evaluating the integral

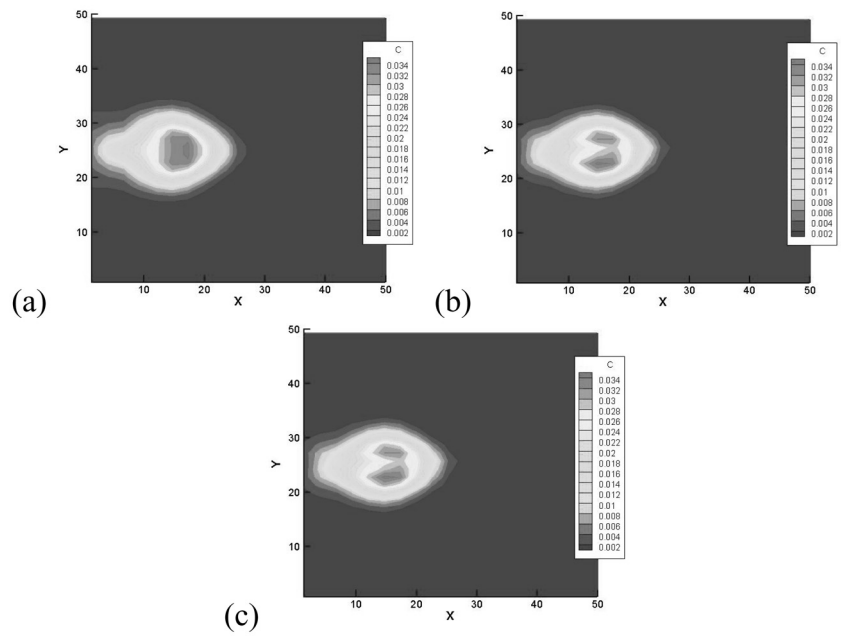

Fig. 1. Plume concentrations: (a) Euler, (b) NS, (c) NS + Turbulence.

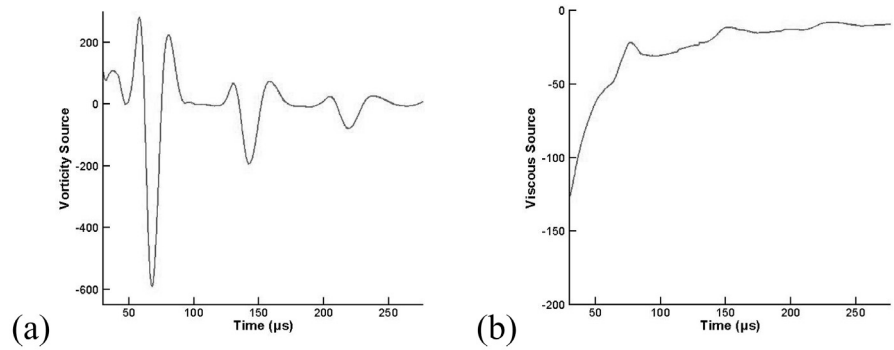

Fig. 2. (a) Vorticity source, (b) viscous diffusion of vorticity.

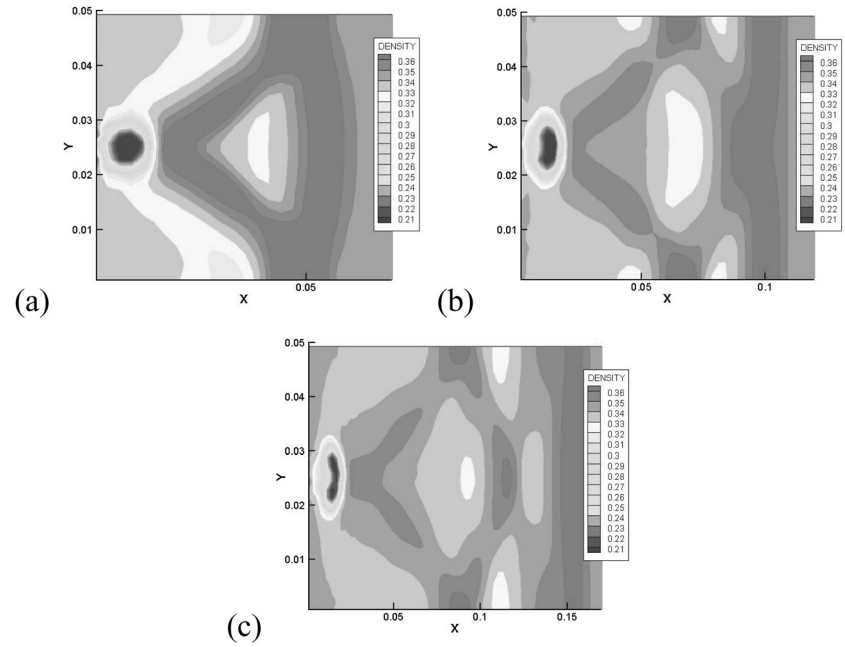

Fig. 3. Density contours at (a) $t = 68\,\mu$s, (b) $t = 140\,\mu$s, (c) t $= 220\,\mu$s.

$$\int\int \frac{1}{\rho_{avg}^2}\left(\frac{\partial\rho}{\partial x}\frac{\partial p}{\partial y}-\frac{\partial\rho}{\partial y}\frac{\partial p}{\partial x}\right)dA \tag{11}$$

where the area of integration is the upper half region of plume with plume concentration greater than 2%. The three peaks corresponding to time moments of interaction of reflected shock waves with the plume are clearly visible in Fig. 2(a). At the corresponding time moments, the density field is shown in Fig. 3. The interaction of reflected shock waves with the plume is clearly seen.

The second term on the r.h.s. of Eq. (10) represents the viscous diffusion of vorticity. It is calculated by evaluating the integral

$$\mu\int\int \frac{1}{\rho_{avg}^2}\left(\frac{\partial^2\omega}{\partial x^2}+\frac{\partial^2\omega}{\partial y^2}\right)dA \tag{12}$$

where the area of integration is same as the area for source term. This source term is plotted in Fig. 2(b) which shows that viscous diffusion of vorticity, as time evolves, attains a fairly stable value. Although this value is smaller than the peaks of the baroclinic vorticity source term, the viscous source term adds vorticity to the plume at all time moments and eventually the viscous effect becomes dominant.

Both terms, the vorticity source and viscous diffusion of vorticity, depend on the injection velocity and on the

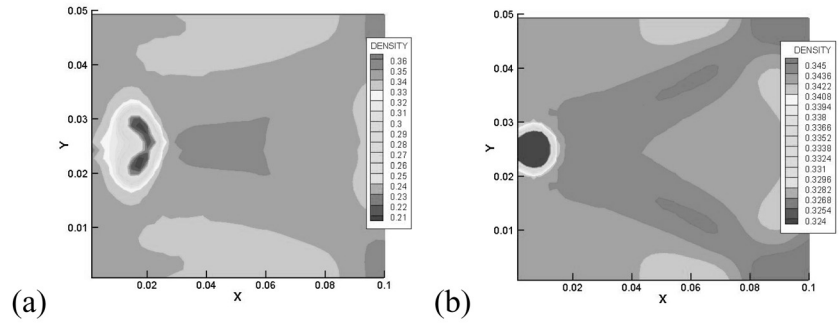

Fig. 4. Density contours (a) high injection velocity, (b) low injection velocity.

base flow conditions. The parameters of the flow and injection velocity determine the distance between the plume and strong shock waves. At higher injection velocities the plume penetrates the reflected shock wave, giving rise to a baroclinic vorticity source and, as a result, the plume immediately turns into the downwards-moving pair as seen in Figure 4.

4. Conclusion

The numerical simulations have captured the basic features of ablation plume. The vorticity source term plays a prominent role at earlier stages of plume evolution. In conducted simulations, the role of viscosity in plume formation is comparable with the baroclinic generation of vorticity for longer simulation times of plume evolution. During the initial time of plume evolution the effect of turbulence on plume evolution is less prominent than viscous and baroclinic effects. However, turbulence may affect the plume evolution in its later stages when its speed of propagation slows down.

References

[1] Kelly R, Miotello A, Mele A, Guidoni AG. Plume formation and characterization in laser-surface interactions. Exp Methods Phy Sci 1998;30:225–289.

[2] Puretzky A, Schittenhelm H, Fan X, Lance M, Allard L, Geohegan D. Investigation of single-wall carbon nanotube growth by time-restricted laser vaporization. Phys Rev B 2002;65 245425–245425–9.

[3] Anisimov SI, Bauerle D, Lukyanchuk BB. Gas dynamics and film profiles in pulsed-laser deposition of materials. Phys Rev B 1993;48:12076–12081.

[4] Mao SS, Mao X, Grief R, Russ RE. Influence of preformed shock wave on the development of picosecond laser ablation plasma. J Appl Phys 2001; 89:4096–4099.

[5] Lobao D, Povitsky A. Furnace geometry effects on plume dynamics in laser ablation. Math Comput Simulation (Special Issue on Wave Propagation) 2004;65:365–383. Short version in Proc of ICCSA-2003, Lecture Notes in Computer Science 2668 2003, pp. 871–880.

[6] Lobao D, Povitsky A. Single and multiple plume dynamics in laser ablation for nanotube synthesis. AIAA J 2004 (accepted), short version, AIAA Paper, 2003–3923, 2003.

[7] Quirk JJ, Karni S. On the dynamics of a shock-bubble interaction. J Fluid Mech 1996;318:129–163.

[8] Greendyke R, Scott C, Swain J. CFD simulation of laser ablation in carbon nanotube production. In AIAA Paper 2002–3026, June 2002.

[9] Bulgakov AV, Bulgakova NM. Gas-dynamic effects of the interaction between a pulsed laser ablation plume and the ambient gas: analogy with an under-expanded jet, J Phys D Appl Phy 1998;31:693–703.

[10] Shu CW. Essentially non-oscillatory and weighted essentially non-oscillatory schemes for hyperbolic conservation laws. NASA/CR-97-206253, 1997.

[11] Povitsky A, Salas M. Thermal regime of catalyst particles in reactor for production of carbon nanotubes. AIAA J 2003; 41(11):2130–2142.

[12] Puretzky A, Geohegan D, Fan X, Pennycook S. Dynamics of single-wall carbon nanotube synthesis by laser vaporization. Appl Phys A 2000; 70:153–160.

[13] Yang J, Kubota T, Zukoski E. A model for characterization of a vortex pair formed by shock passage over a light-gas inhomogenity. J Fluid Mech 1994;258:217–244.